Materials Science & Engineering A 585 (2013) 480–487

Contents lists available at ScienceDirect

Materials Science & Engineering A

journal homepage: www.elsevier.com/locate/msea

Effect of solution heat treatment on the internal architecture and compressive strength of an AlMg4.7Si8 alloy

D. Tolnai [a,b,*], G. Requena [a], P. Cloetens [c], J. Lendvai [b], H.P. Degischer [a]

[a] Institute of Materials Science and Technology, Vienna University of Technology, Karlsplatz 13/308, A-1040 Vienna, Austria
[b] Eötvös Loránd University, Department of Materials Physics, POB 32, H-1518 Budapest, Hungary
[c] European Synchrotron Radiation Facility, 6 Rue Jules Horowitz, F-38000 Grenoble Cédex, France

ARTICLE INFO

Article history:
Received 12 March 2013
Received in revised form
3 June 2013
Accepted 8 June 2013
Available online 20 June 2013

Keywords:
Al alloys
Coarsening
Synchrotron radiation computed tomography
3D characterization
Load transfer

ABSTRACT

The evolution of the microstructure of an AlMg4.7Si8 alloy is investigated by scanning electron microscopy and ex situ synchrotron tomography in as-cast condition and subsequent solution treatments for 1 h and 25 h at 540 °C, respectively. The eutectic Mg_2Si phase, which presents a highly interconnected structure in the as-cast condition, undergoes significant morphological changes during the solution heat treatment. Statistical analyses of the particle distribution, the sphericity, the mean curvatures and Gaussian curvatures describe the disintegration of the interconnected seaweed-like structure followed by the rounding of the disintegrated fractions of the eutectic branches quantitatively. The ternary eutectic Si resulting from the Si-surplus to the stoichiometric Mg_2Si ratio of the alloy undergoes similar changes. The morphological evolution during solution heat treatment is correlated with results of elevated temperature compression tests at 300 °C. The elevated temperature compressive strength is more sensitive to the degree of interconnectivity of the three dimensional Mg_2Si network than to the shape of the individual particles.

1. Introduction

Cast AlMgSi alloys are potential candidates for application in the automotive and aerospace industries [1]. They contain α-Al dendrites, primary Mg_2Si particles, α-Al/Mg_2Si eutectic, and aluminides originating from Fe and Mn casting impurities [2]. These phases are complemented with a ternary eutectic, formed by α-Al, Mg_2Si and Si in case of a Si surplus to the stoichiometric Mg:Si ratio (1.74:1) in the alloy [2,3].

Several experimental methods have been utilized to characterize the microstructures in alloys of this system, such as calorimetry [4], crystallography [5,6], and imaging [7]. Two-dimensional (2D) metallographic investigations revealed that the Mg_2Si phase exhibits a so-called 'Chinese-script' morphology, while the Fe- and Mn-intermetallics appear needle-like on the images [3]. On the other hand, three-dimensional (3D) metallography shows that the eutectic Mg_2Si has a spatially extended, highly interconnected coral-like structure, while the shape of the Fe- and Mn-aluminides ranges from needle- to platelet-like [8,9] depending on the space available in the interdendritic region during solidification [10,11]. The internal architecture of multiphase alloys, i.e. the volume fraction and spatial arrangement of the microstructural phases, plays a vital role in determining their strength [12]. Therefore, the quantification of morphological parameters such as interconnectivity of phases or contiguity between them [13] is essential to understand the macroscopic behaviour of these alloys [14]. Although the extrapolation from 2D to 3D is restrictively possible by assuming statistically uniform distribution of phases [15], 3D imaging methods are necessary if the phases are non-uniformly distributed, have complex morphologies, form interconnected structures and/or contiguity is present between those structures [16,17].

Synchrotron-based microtomography is a unique non-destructive tool in materials science. Due to the high brilliance of the source and the transversal coherence of the beam [18], a wide range of multiphase materials can be imaged [8,9,12,19–22]. The transversal coherence of the beam can be exploited to produce phase contrast in cases when different constituting phases have similar X-ray attenuations [23]. Furthermore, phase retrieval (e.g. holotomography [24]) can be performed for accurate quantitative analysis.

The aim of this study is to describe the internal architecture of an as-cast AlMg4.7Si8 alloy, to follow the changes of the

* Corresponding author. Current address: Magnesium Innovation Centre MagIC, Helmholtz-Zentrum Geesthacht, Max Planck Straße 1., D-21502 Geesthacht, Germany. Tel.: +49 4152 871974; fax: +49 4152 871909.
E-mail address: domonkos.tolnai@hzg.de (D. Tolnai).

0921-5093
http://dx.doi.org/10.1016/j.msea.2013.06.033

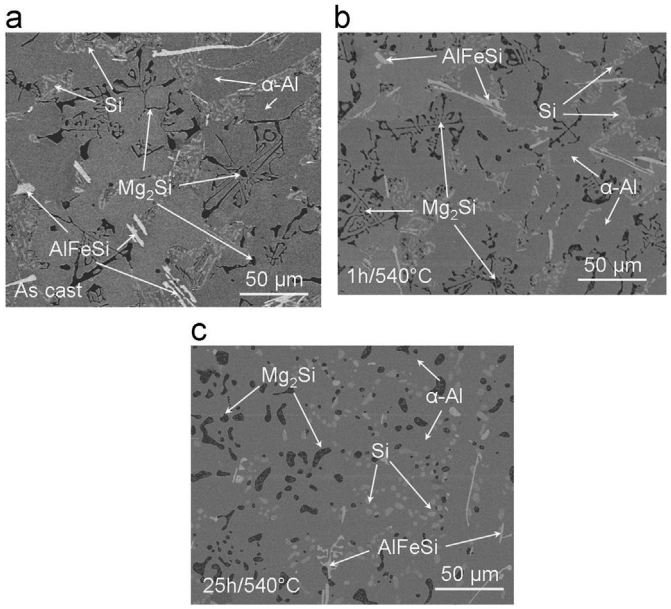

Fig. 1. BSE micrographs of AlMg4.7Si8 in (a) as-cast condition, (b) after 1 h at 540 °C and (c) after 25 h at 540 °C.

microstructural morphology in 3D after subsequent 1 h and 25 h at 540 °C solution heat treatments of the same samples and to link these changes to the elevated temperature strength determined by compression tests.

2. Experimental methods

2.1. Material

An AlMg4.7Si8 alloy produced by gravity die casting was investigated. The Mg:Si ratio for this composition is 0.58:1, which is lower than that of the stoichiometric Mg_2Si compound [2,3]. The microstructure consists of α-Al dendrites, a binary α-Al/Mg_2Si eutectic, a ternary α-Al/Mg_2Si/Si eutectic and Fe-aluminides originating from Fe impurity (Fe ~0.5 wt%) [3]. This is shown for the alloy in as-cast condition in the backscattered electron (BSE) micrograph in Fig. 1(a). The indicated phases were identified by energy dispersive X-ray spectroscopy. Cylindrical specimens with a length of 10 mm and 1 mm diameter were used for synchrotron tomography.

2.2. Elevated temperature compression tests

Elevated temperature compression tests were carried out at 300 °C, controlled by a type *K* thermocouple, using a Gleeble 1500 servo hydraulic system machine at an initial strain rate of 1.25×10^{-3} s^{-1}. The alloy was tested in as-cast condition, after 1 h and 25 h at 540 °C, respectively, using the same samples with cylindrical geometry of 10 mm length and 5 mm diameter. Prior to the tests, the samples were subjected to an overaging heat treatment at 300 °C during 2 h to stabilize the precipitation condition and to minimize the overlapping strengthening effect of Mg_2Si precipitates. This overaging heat treatment does not alter the morphology of the eutectic Mg_2Si and Si particles [9].

2.3. Scanning electron microscopy

Scanning electron microscopy (SEM) was performed with a Philips XL30 device and a FEI Quanta 200 Field Emission Gun SEM (FEG-SEM). Deep etching of the Al was performed for 5 min using a 1:10 $NaOH/H_2O$ solution to reveal the spatial architecture of the other phases.

2.4. Tomography

The samples were imaged at the ID19 beamline of the European Synchrotron Radiation Facility [18] using a beam energy of 29 keV and a sample-to-detector distance of 29 mm. 1500 Radiographies were acquired between 0° and 180° during the scans. The ESRF FReLoN (Fast Readout Low Noise) camera [25] with an effective pixel size of 0.28 μm was used to acquire the radiographies. The exposure time was 1 s/projection for the same sample at different conditions. After the first tomography of the alloy in as-cast condition the sample was subjected to a solution heat treatment of 1 h at 540 °C before the second tomography, and subsequently to 24 h at 540 °C before the tomographic scan at the final stage. The size of the reconstructed 32 bit volumes was 2048^3 voxel with a voxel size of $(0.28\ \mu m)^3$.

2.5. Image processing

The same $1200 \times 1050 \times 975$ voxel volume was selected as the region of interest from the reconstructed tomographic volumes in as-cast and solution heat treated conditions. The volumes were subjected to a 2D Gaussian filter in ImageJ [26] with a mask radius of 2. The 32 bit volumes were converted to 8 bit within grey-value histogram limits of −1.5 and 1.5. The different phases were segmented by global thresholding and applying a region growing algorithm which is based on the grey level of the voxels [27]. Morphological smoothing was then applied: voxels outside of the segmented region but connected to it by four or more faces of the cubic voxels were added to the segmented phase. On the other hand, segmented voxels at the edge of the segmented region attached only by one face were removed. Only particles larger than 27 voxels (~0.6 μm³) were considered for evaluation.

2.6. Morphological parameters

Morphological parameters have been calculated to quantify changes of the microstructure during solution heat treatment.

2.6.1. Sphericity

The sphericity, C_p, is calculated according to (1), where *V* and *S* are the volume and the surface of a given particle, respectively (see e.g. [28]). Thus, $C_p=1$ corresponds to a sphere, while $C_p=0$ to an infinite plate.

$$C_p = \frac{6\pi^{1/2}V}{S^{3/2}} \quad (1)$$

2.6.2. Interconnectivity

The interconnectivity of a phase, I, is defined in this work as the volume of the largest individual particle (particle=continuous 3D region of the corresponding phase) of the investigated phase, $V_{f\ larg}$, divided by the total volume of thein the analyzed volume, V_f

$$I = \frac{V_{f\ larg}}{V_f} \quad (2)$$

2.6.3. Curvatures

The mean (*K*) and Gauss curvatures (*H*), defined as the mean and the product of the principal curvatures, respectively, were determined for the eutectic Mg_2Si using the software Avizo® [29]. A detailed description of the calculation can be found in [10].

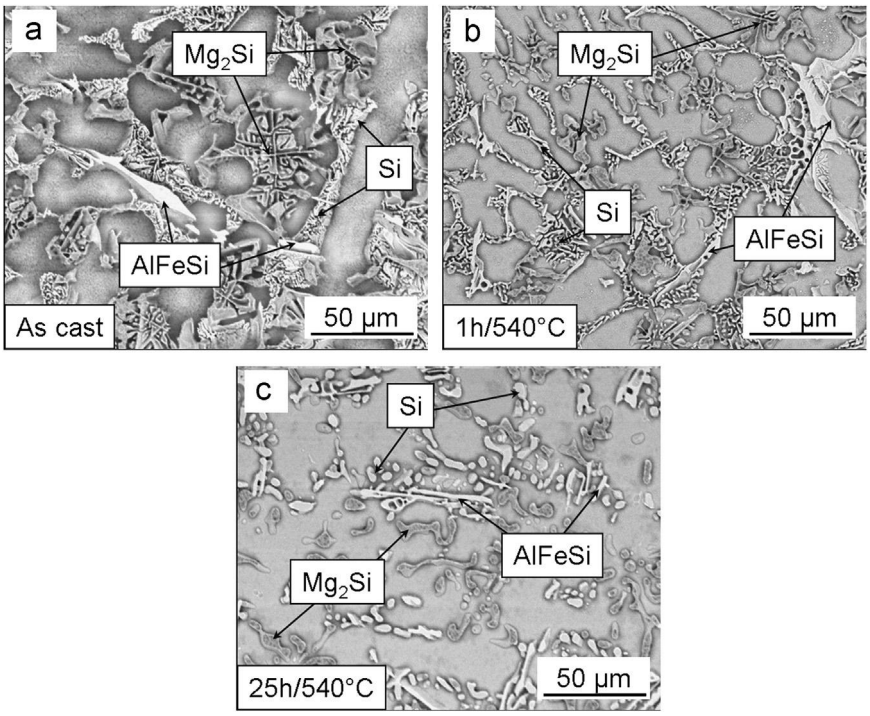

Fig. 2. BSE micrographs of the rigid phases revealed by deep etching the α-Al matrix in (a) as-cast condition, (b) after 1 h at 540 °C and (c) after 25 h at 540 °C.

3. Results

3.1. Electron microscopy

BSE micrographs of AlMg4.7Si8 in as-cast, 1 h at 540 °C and 25 h at 540 °C conditions are shown in Fig. 1. Slight spheroidization of the Mg_2Si and Si particles can be observed after 1 h solution heat treatment (Fig. 1b). The AlFeSi particles do not undergo observable morphological changes for the same condition. The 25 h solution heat treatment results in a pronounced spheroidization of the Mg_2Si and Si phases (Fig. 1c). Furthermore, the AlFeSi particles also undergo a slight spheroidization. Some contiguity remains between the Mg_2Si and the Si phases. The spheroidization of the eutectic particles can be followed more clearly after deep etching of the Al, as shown in Fig. 2. Moreover, the deep etched topography of the alloy after 25 h solution treatment presents cup-like marks where particles have fallen out during etching (Fig. 2c), which indicate the disintegration of the interconnected eutectic phases.

3.2. Synchrotron tomography

Cropped tomographic slices of approximately the same region are shown in Fig. 3(a)–(c) for the as-cast and solution heat treated conditions, respectively. Similarly to the micrographs shown in Fig. 1, the tomographic slices show that the eutectic Mg_2Si structure coarsens and spheroidizes during the solution heat treatment, while the AlFeSi phase, unrevealed by the 2D results, seems to dissolve partially.

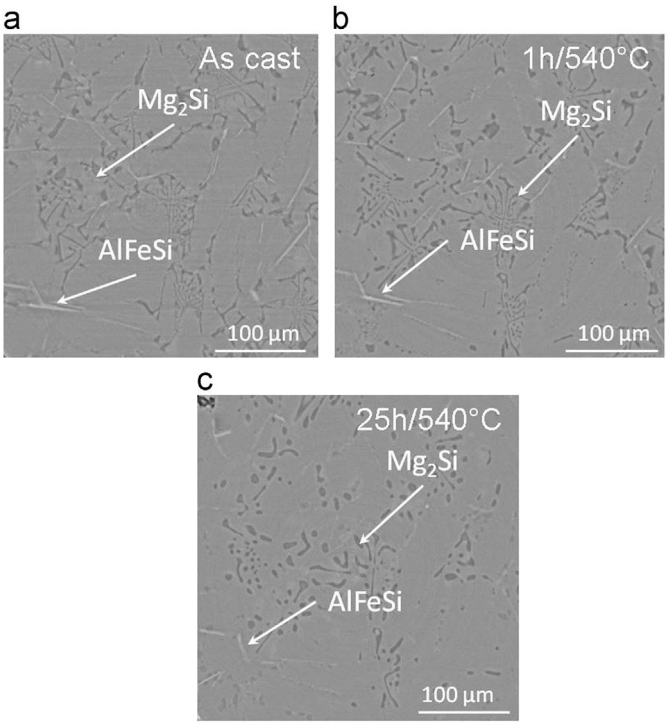

Fig. 3. Reconstructed tomographic slices in (a) as-cast condition, (b) after 1 h at 540 °C and (c) after 24 h at 540 °C. The voxel size is $(0.28\ \mu m)^3$.

3.2.1. Mg_2Si

Rendered volumes of the segmented Mg_2Si phase are shown in Fig. 4(a)–(c) for the same sub-volume of $275 \times 300 \times 335\ \mu m^3$ in the as-cast and the solution heat treated conditions, respectively. The different colours represent unconnected particles within this sub-volume. The largest Mg_2Si particle in each condition is shown separately. The loss of interconnectivity with increasing solution treatment time is clearly revealed by the decrease in size of this largest particle.

The evolution of the number of particles and the relative volume fraction of the largest particle (interconnectivity) of the Mg_2Si phase in the same sub-volumes as shown in Fig. 4 are listed in Table 1. The number of the Mg_2Si particles increases by a factor of 4 in the first hour of the heat treatment followed by a further increase by ~55% in the next 24 h. The interconnectivity is 87%

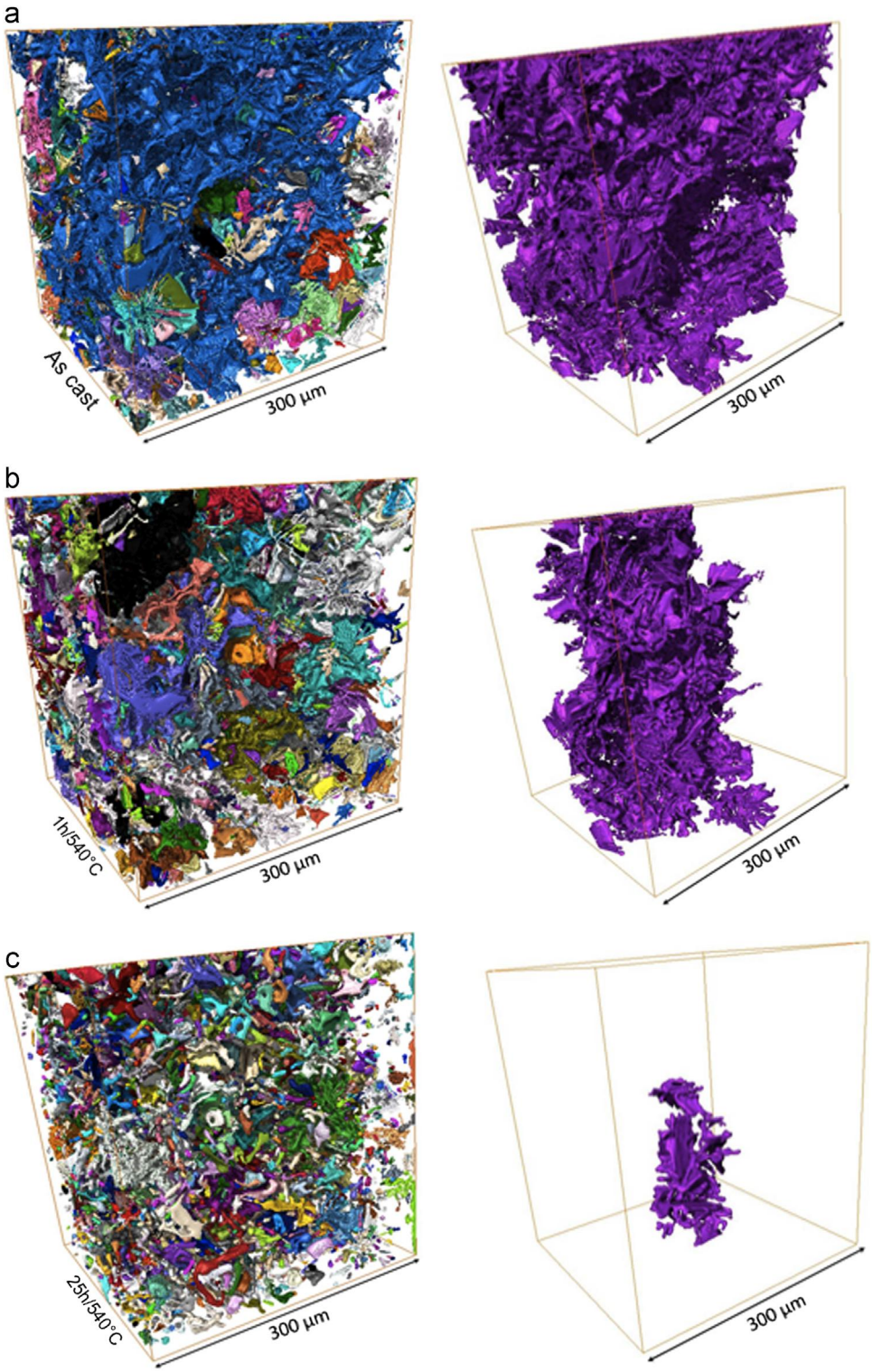

Fig. 4. Rendered tomographic volumes of the Mg_2Si phase and the largest particle in the same $275 \times 300 \times 335\ \mu m^3$ region in: (a) as-cast condition, (b) after 1 h at 540 °C and (c) after 25 h at 540 °C. The different colours indicate unconnected particles within the studied volume. The voxel size is $(0.28\ \mu m)^3$.

within the investigated sub-volume in the as-cast condition. It decreases to 57% after 1 h at 540 °C and further to 3.5% after 25 h at 540 °C.

The evolution of the sphericity of the Mg_2Si particles in the sub-volume shown in Fig. 4 is presented in Fig. 5. The distribution of the sphericity shifts to higher values after 25 h at 540 °C indicating that the particles transform into more spheroid-like shapes. The mean value of the distribution in the as-cast condition is 0.43 ± 0.2 and does not change after 1 h at 540 °C but increases to 0.63 ± 0.2 after 25 h at 540 °C.

The distribution of the surface curvatures is shown in Fig. 6 as a 2D histogram. This representation combines the mean and the Gauss curvatures for each surface part and provides information on real shapes [30]. In the as-cast condition (Fig. 6a) there is a

Table 1
Quantitative parameters obtained from the synchrotron tomography volumes shown in Fig. 4 and 7 of the AlMg4.7Si8 alloy in as-cast and solution heat treated conditions.

	As-cast	1 h at 540 °C	25 h at 540 °C
Mg_2Si			
Number of particles	849	3343	5199
Volume fraction V_f (%)	10	11	11
Volume of the largest particle (μm^3)	2.9E6	2.2E6	1.38E5
Relative V_f and (V_f) of the largest particle (%)	87 (8.7)	57 (6.6)	3.5 (0.4)
AlFeSi			
Number of particles	54	49	80
Volume fraction V_f (%)	0.9	0.82	0.34
Volume of the largest particle (μm^3)	92936	68673	9959
Relative V_f and (V_f) of the largest particle (%)	31 (0.28)	25 (0.2)	8 (0.03)

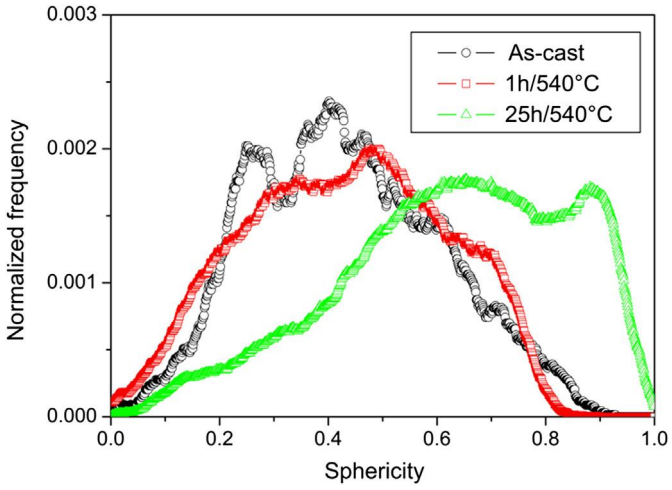

Fig. 5. Sphericity distributions of the Mg_2Si particles in as-cast and solution heat treated conditions.

maximum of the normalized distribution located close to the origin in the negative part of the Gauss curvature domain, which indicates a large population of symmetric saddle-like surfaces. The frequency of this maximum increases after 1 h at 540 °C (Fig. 6b), while the frequency of outer sections tend to decrease resulting in a narrower distribution. After 25 h at 540 °C (Fig. 6c) a second maximum appears in the positive-positive quadrant of the coordinate system indicating the appearance of more spheroidal surfaces. Moreover, the distribution becomes even narrower with the extremes corresponding to smaller radii (larger curvatures) tending to disappear.

3.2.2. AlFeSi

The segmented AlFeSi phase in as-cast and solution heat treated conditions is shown in Fig. 7 for the same volume as in Fig. 4. The different colours represent unconnected particles within the investigated sub-volume. Based on the colour codes there are two large particles present in as-cast condition (light-blue and yellow) which resist up to some extent the solution heat treatment for 1 h at 540 °C (the particles are now shown green and brown in Fig. 7b). The volume fraction of this phase decreases from 0.9 vol% in as-cast condition to 0.82 vol% after 1 h at 540 °C, while the level of interconnectivity decreases from 31% to 25%. After 25 h at 540 °C, the volume fraction and interconnectivity decrease further to 0.34 vol% and 8%, respectively (Table 1).

3.3. Elevated temperature compression tests

The stress–strain curves of compression tests at 300 °C are shown in Fig. 8. Strain hardening is observed for all conditions until the maximum stress is reached followed by a softening period. The proof stress $\sigma_{0.2}$ decreases from 67 ± 0.5 MPa in as-cast condition to 52 ± 4 MPa after 1 h at 540 °C and to 50 ± 2 MPa after 25 h at 540 °C. The maximum strength shows a decrease from 76 ± 2 MPa in as-cast condition to 61 ± 1 MPa after 1 h at 540 °C, and further to 57 ± 1 MPa after 25 h at 540 °C. The $\sigma_{0.2}$ and maximum strength values were obtained as the mean of the two tested samples per condition, while the deviation is only a rough estimation calculated as the difference of the actual values to their mean.

4. Discussion

4.1. Iron aluminides

The AlFeSi phase undergoes a slight spheroidization, as evident from the etched microstructures in Fig. 2 and a decrease in the volume fraction from 0.9 to 0.34 vol% after 25 h of solution heat treatment at 540 °C (see Table 1). On one hand, this can be related to dissolution of particles formed as a consequence of segregation during solidification and, on the other hand, a phase transformation may also occur [2]. Three stable aluminide phases can be present in the Al–Mg–Si–Fe system: α-Al_8Fe_2Si, β-Al_5FeSi and δ-$Al_8FeMg_3Si_6$. A transformation of β-Al_5FeSi into α-Al_8Fe_2Si reduces the volume fraction of the Fe-aluminides for a given Fe-concentration. If the α- or β-AlFeSi particles transform into δ-$Al_8FeMg_3Si_6$ [31], the uptake of Mg decreases the X-ray absorption contrast of the aluminide particles with respect to the α-Al matrix [32], causing a segmentation problem. Since the volume fraction of the Fe-aluminides is below 1 vol% and marginal contiguity was found between the AlFeSi-phases and eutectic particles, their reinforcing contribution to the macroscopic strength can be considered as negligible [33,34].

4.2. Si in the ternary eutectic

The disintegration and the rounding of the Si phase owing to diffusion driven spheroidization (see e.g. [12]) can be observed in the micrographs shown in Figs. 1 and 2 parallel to the morphological changes occurring in the Mg_2Si phase. The contiguity observed in as-cast condition remains unchanged after solution treatment, suggesting that the interface energy between Mg_2Si and Si is lower than between Al and Si [35].

4.3. Eutectic Mg_2Si

The eutectic Mg_2Si undergoes morphological changes similar to those observed for the eutectic Si during solution heat treatment of cast Al–Si alloys [9], which can be described by the diffusion controlled spheroidization of the architecture of this phase. It has been proposed that the spheroidization of Si takes place in two steps: first, the disintegration of the structure at thinner sections of the eutectic particles and, second, the further rounding of disintegrated particles [36]. This process can be followed from the morphological analysis in the present work: in the first hour of solution heat treatment, an increase of symmetric saddle-like surfaces takes place as shown by the curvature analysis in Fig. 6

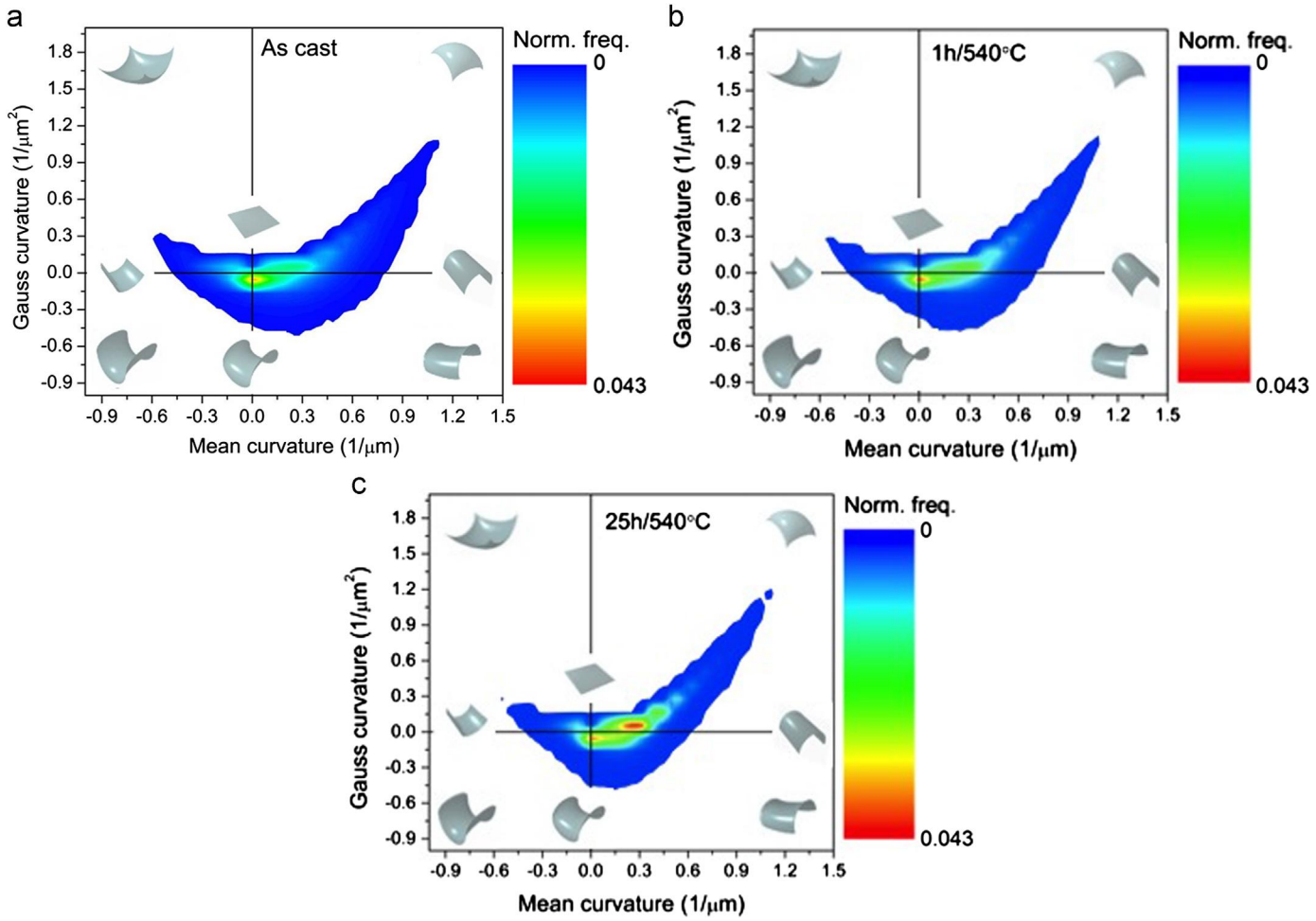

Fig. 6. Curvature distribution of the Mg_2Si phase in (a) as-cast condition, (b) after 1 h at 540 °C and (c) after 25 h at 540 °C.

(b), that is an indication of neck formation resulting in a larger fraction of necks. Furthermore, it is seen that the number of Mg_2Si particles increased in the same time period by a factor of 4 (see Table 1), while the sphericity of this phase remains practically unchanged (see Fig. 5). These three facts imply that the main morphological process during the first hour of solution treatment is the fragmentation of the larger Mg_2Si particles by pinching off the thinner arms.

In the following 24 h of solution heat treatment, the number of Mg_2Si particles increases further by a factor of 1.5, indicating a further but slower fragmentation of the Mg_2Si structure. On the other hand, the fraction of symmetric saddle-like surfaces decreases, while the fraction of spheroidal surfaces increases as reflected by the appearance of a new maximum in the curvature distribution (see Fig. 6c). These two facts, together with the prominent shift of the sphericity distribution towards one indicate that the dominant morphological change between 1 h and 25 h of solution treatment time is the rounding of disconnected Mg_2Si particles.

4.4. Correlation between the internal architecture and compressive strength at elevated temperature

A decrease of the elevated temperature compressive strength with solution heat treatment time can be observed for the investigated AlMg4.7Si8 alloy in over aged condition. This is similar to the case of eutectic Al–Si alloys [37], where the load transfer from the α-Al matrix to the rigid eutectic Si determines the strength. The load carrying capability of the eutectic Si is given by its volume fraction, size, morphology, connectivity, spatial distribution and mechanical properties (see e.g. [14,38]). It was shown recently that depending on its architecture the Mg_2Si phase can also act as a reinforcement in AlMgSi alloys [9]. The as-cast microstructure of the AlMg4.7Si8 alloy studied in this work is characterized by a high level of interconnectivity of the largest Mg_2Si particle (87%—Table 1). This suggests that the strength in this condition is largely determined by the reinforcing effect of this single particle, which amounts to 8.7 vol%. To assess the effect of sphericity on strength, in the 1 h and 25 h solution treated conditions only the largest Mg_2Si particles the volume fraction of which sum upto 8.7 vol%, are considered. Thus, the mean sphericity of 1 Mg_2Si particle in as-cast condition, 119 after 1 h at 540 °C and 1436 after 25 h at 540 °C is correlated with the elevated temperature strength. Fig. 9 shows the evolution of σ_{max} and $\sigma_{0.2}$, of the interconnectivity of Mg_2Si and of the mean sphericity of the largest Mg_2Si particles (amounting 8.7 vol%) with solution treatment time. It can be seen that the strength of the alloy decreases by about 20% in the first hour of solution heat treatment and then remains practically constant during further exposure to 540 °C. The comparison with the morphological changes shows, that the dominant microstructural process is the partial loss of interconnectivity (from 87 to 57%) in the period of the initial drop in strength, while the shape of the individual particles (mean sphericity) remains practically

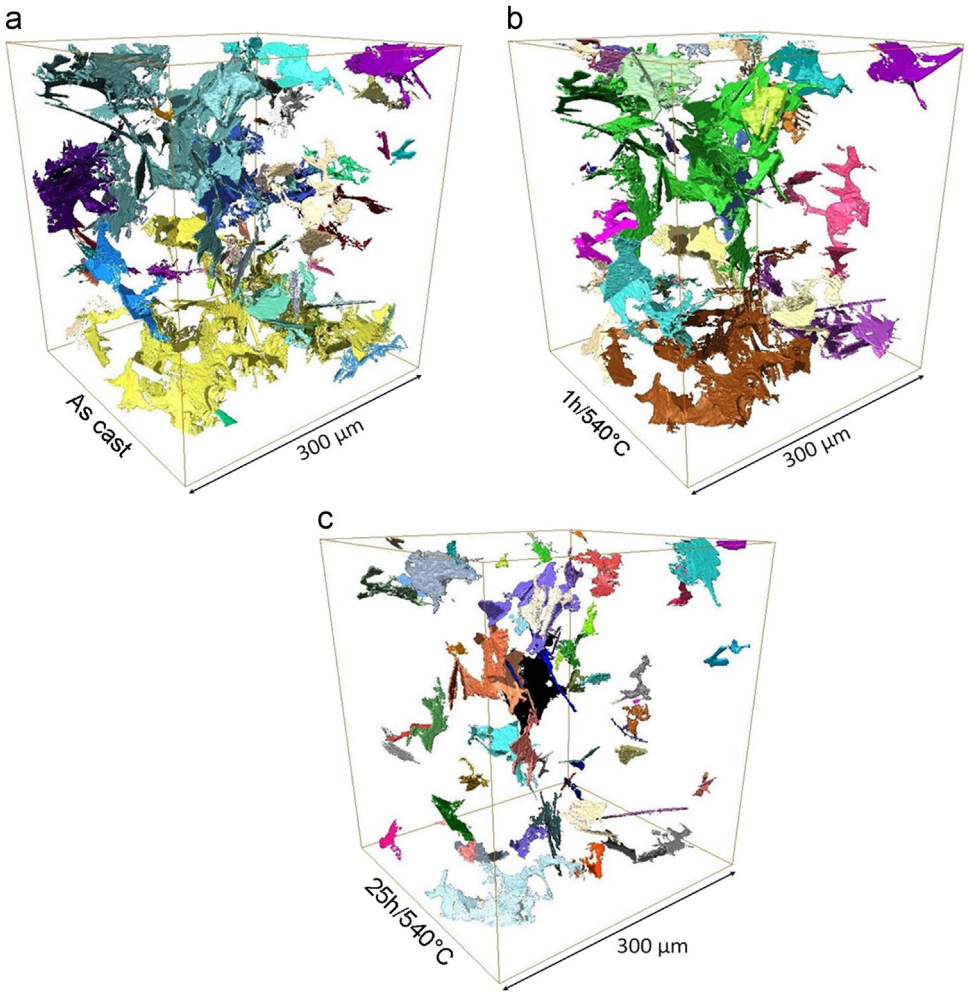

Fig. 7. Rendered tomographic volumes of the AlFeSi phase in the same 275 × 300 × 335 μm^3 region as shown in Fig. 4 in (a) as-cast condition, (b) after 1 h at 540 °C and (c) after 25 h at 540 °C. The different colours indicate unconnected particles within the studied volume. The voxel size is (0.28 $\mu m)^3$.

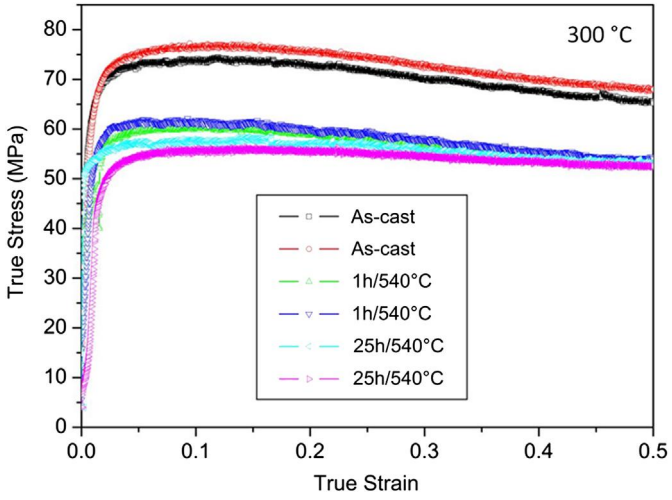

Fig. 8. Stress–strain curves of compression tests at 300 °C.

unchanged, but increases with prolonged solution treatment. This implies that the high degree of interconnectivity (close to 1) of the 3D network of Mg_2Si has a predominant influence on the elevated temperature strength of the alloy in comparison to the shape of individual particles disconnected by solution heat treatment.

5. Conclusions

The microstructural changes in a gravity cast AlMg4.7Si8 alloy during solution heat treatment at 540 °C have been investigated by scanning electron microscopy and synchrotron tomography. Their influence on elevated temperature compressive strength can be explained as follows:

- The as-cast alloy contains a highly interconnected 3D network of Mg_2Si of 10 vol% with a coral-like morphology presenting some contiguity with eutectic Si and, to a less extent, with the platelet-like Fe-containing aluminides of 1 vol%.
- The solution heat treatment results in a diffusion controlled spheroidization of the Mg_2Si phase that evolves in the following two stages: the loss of interconnectivity by pinching off arms of the larger Mg_2Si particles dominates in the first hour, slowing down afterwards. Further rounding of the disconnected particles becomes relevant in the subsequent 24 h of solution heat treatment.
- The compressive strength ($\sigma_{0.2}$, σ_{max}) at 300 °C decreases by about 20% after 1 h at 540 °C and remains practically constant at that level during subsequent solution treatment. The

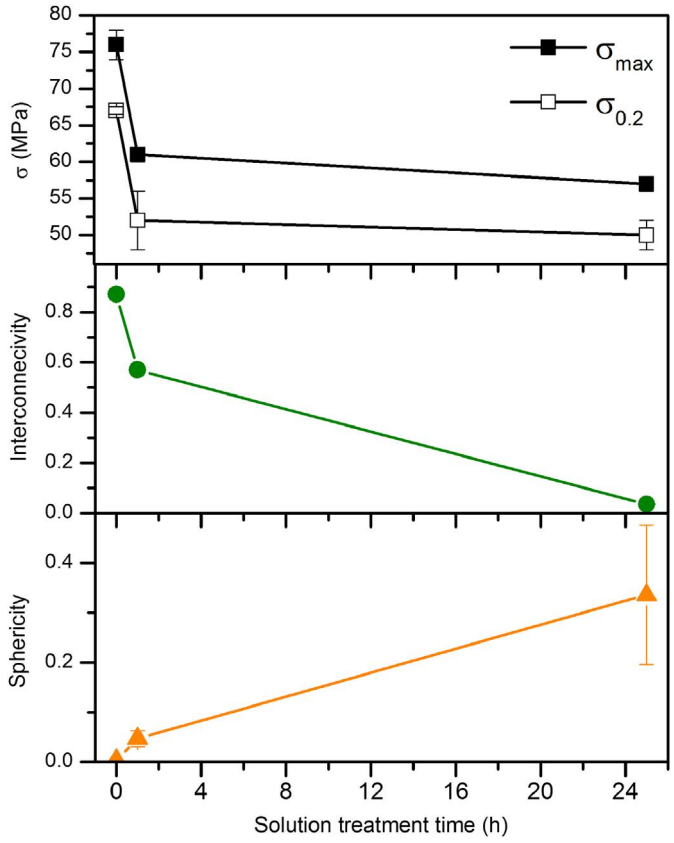

Fig. 9. Elevated temperature compressive strength, interconnectivity and mean sphericity of the largest Mg_2Si particles amounting to 8.7 vol% in each condition.

correlation with the morphological analysis shows that the partial loss of interconnectivity of the Mg_2Si phase is the dominant reason for the drop in strength within a short period of solution treatment, while the shape, described by the mean sphericity of the larger particles, increases continuously with solution treatment time. This indicates that the elevated temperature compressive strength is more sensitive to the interconnectivity of the Mg_2Si architecture than to the shape of the individual particles.

Acknowledgements

The authors would like to thank the European Synchrotron Radiation Facility for the provision of synchrotron radiation facilities in the framework of proposal MA505. The University Service for Transmission Electron Microscopy (USTEM) of the Vienna University of Technology is acknowledged for the provision of the field emission gun scanning electron microscope. D. Tolnai, G. Requena and H.P. Degischer are grateful to the Austrian Science Found (FWF P22876-N22, FWF L 588-N14) and to the Austrian Agency for International Cooperation (WTZ HU 03/2010). D. Tolnai and J. Lendvai acknowledge the Hungarian Research Fund (OTKA-K-67692) and the Hungarian Research and Technology Foundation (TET AT-12/2009).

References

[1] F. Ostermann, Anwendungstechnologie Aluminium, Springer Verlag, Berlin Heidelberg, 2007.
[2] L.F. Mondolfo, Al Alloys: Structures and Properties, Butterworth-London, Boston, 1976.
[3] H.P. Degischer, H. Knoblich, J. Knoblich, E. Maire, L. Salvo, M. Suéry, Sonderb. Prakt. Metallogr. 38 (2006) 67–74.
[4] H.B. Dong, R. Brooks, Mater. Sci. Eng. A 413–414 (2005) 480–484.
[5] M.V. Kral, H.R. McIntyre, M.J. Smillie, Scri. Mater. 51 (2004) 215–219.
[6] M.V. Kral, Materials Letters 59 (2005) 2271–2276.
[7] C. Li, Y. Wu, H. Li, X.F. Liu, Acta Materialia 59 (2011) 1058–1067.
[8] F. Lasagni, A. Lasagni, M. Engstler, H.P. Degischer, F. Müklich, Advanced Engineering Materials 10 (2008) 62–66.
[9] D. Tolnai, G. Requena, P. Cloetens, J. Lendvai, H.P. Degischer, Materials Science and Engineering A 550 (2012) 214–221.
[10] D. Tolnai, P. Townsend, G. Requena, J. Lendvai, H.P. Degischer, Acta Materialia 60 (2012) 2568–2577.
[11] S. Terzi, J.A. Taylor, Y.H. Cho, L. Salvo, M. Suéry, E. Boller, Acta Materialia 58 (2010) 5370–5380.
[12] G. Requena, G. Garcés, M. Rodriguez, T. Pirling, P. Cloetens, Adv. Eng. Mater. 11 (2009) 1007–1014.
[13] Z. Asghar, G. Requena, H.P. Degischer, P. Cloetens, Acta Mater. 57 (2009) 4125–4132.
[14] G. Requena, G. Garcés, Z. Asghar, E. Marks, P. Staron, P. Cloetens, Advanced Engineering Materials 13 (2011) 674–684.
[15] A. Velichko, F. Mücklich, Praktische Metallographie/Practical Metallography 45 (2008) 423–439.
[16] C.F. Mora, A.K.H. Kwan, Cement and Concrete Research 30 (2000) 351–358.
[17] M.V. Kral, M.A. Mangan, G. Spanos, R.O. Rosenberg, Materials Characterization 45 (2000) 17–23.
[18] European Synchrotron Radiation Facility; ⟨http:/esrf.eu⟩.
[19] D. Fuloria, P.D. Lee, P.D. Bernard, Mater. Sci. Eng. A 494 (2008) 3–9.
[20] G. Requena, H.P. Degischer, E. Marks, E. Boller, Mater. Sci. Eng. A 487 (2008) 99–107.
[21] A. Borbély, F.F. Csikor, S. Zabler, P. Cloetens, H. Biermann, Mater. Sci. Eng. A 367 (2004) 40–50.
[22] G. Requena, G. Fiedler, B. Seiser, H.P. Degischer, M. Di Michiel, T. Buslaps, Composites Part A 40 (2008) 152–163.
[23] J. Baruchel, J.Y. Buffiére, E. Maire, P. Merle, G. Peix, X-Ray Tomography in Material Science, HERMES Science Publications, Paris, 2000.
[24] P. Cloetens, W. Ludwig, J. Baruchel, D. Van Dyck, J. Van Landuy, J.P. Guigay, M. Schlenker, Appl. Phys. Lett 75 (1999) 2912–2915.
[25] J.C. Labiche, O. Mathon, S. Pascarelli, M.A. Newton, G.G. Ferre, C. Curfs, G. Vaughan, A. Homs, D.F. Carreiras, Review of Scientific Instruments 78 (2007), art. no. 091301.
[26] ImageJ, ⟨http:/rsbweb.nih.gov/ij/⟩.
[27] tomo3D, ⟨http:/metal.elte.hu/tomo3D⟩.
[28] J. Ohser, F. Mücklich, Statistical Analysis of Micro Structures in Materials Science, John Wiley & Sons Ltd., Chichester, 2000.
[29] Avizo Fire, ⟨http:/vsg3d.com/node/25⟩.
[30] N.C.W. Kuijpers, J. Tirel, D.N. Hanlon, S. van der Zwaag, Materials Characterization 48 (2002) 379–392.
[31] N.A. Belov, D.G. Eskin, A.A. Askenov, Multicomponent Phase Diagrams, Application for Commercial Aluminium Alloys, Elsevier, Oxford, UK, 2005.
[32] X-Ray Oriented Program (XOP). ⟨http:/www.esrf.eu/computing/scientific/xop2.1⟩.
[33] T.W. Clyne, P.J. Withers, An Introduction to Metal Matrix Composites, Cambridge University Press, Trumpington street, Cambridge CB2 1RP, 1993.
[34] C.M. Friend, Journal of Materials Science 22 (1987) 3005–3010.
[35] E. Ogris, A. Wahlen, H. Lüchinger, P.J. Uggowitzer, Light Metals 2 (2002) 263–269.
[36] P.Y. Zhu, Q.Y. Liu, T.X. Hou, AFS Transactions 93 (1985) 609–614.
[37] Z. Asghar, G. Requena, F. Kubel, Materials Science and Engineering A 527 (2010) 5691–5698.
[38] F. Lasagni, J. Acuña, H.P. Degischer, Met. Mater. Trans. A 39 (2008) 1466–1474.